Deuteron Optical-Model Analysis in the Range of 11 to 27 MeV

C. M. PEREY* AND F. G. PEREY
Neutron Physics Division, Oak Ridge National Laboratory, Oak Ridge, Tennessee†
(Received 13 June 1963)

Deuteron elastic scattering angular distributions are analyzed using a simple optical model without spin-orbit potentials. Discrete valleys in the parameter space of the model are found to give a very good description of the data. Two of these regions are used to analyze 52 angular distributions measured for target nuclei with $Z \geq 12$ and deuteron energies in the range of 11 to 27 MeV, with particular emphasis on data at energies of 11.8, 15, and 21.6 MeV. In order to determine the trends of the optical-model parameters as a function of mass number and energy, four different sets of geometrical parameters are used, and only the well depths, real and imaginary, are varied to obtain a best fit to the experimental data. The real well depths show a smooth linear increase as a function of the Coulomb parameter $Z/A^{1/3}$ and a smooth linear decrease as a function of energy. The imaginary well depths show fairly large fluctuations from element to element but no systematic trend as a function of mass number. For all four sets of parameters, the imaginary well depth decreases rapidly for bombarding energies from 11 to 14 MeV and then increases slowly for energies from 15 to 27 MeV.

I. INTRODUCTION

WITH the advent of fast digital computers with large memories, it is now possible to investigate, to a much greater extent than before, a large domain of the optical-model parameter space. Use is made of automatic search programs[1–4] which adjust the parameters of the model so as to minimize the mean-square deviation, χ^2, between theoretical and experimental cross sections. By allowing a sufficient number of parameters of the model to be adjusted by the optical-model search program, it is usually possible to obtain excellent agreement with the data for the elastic scattering of nucleons, deuterons, alpha particles, and even heavy ions. However, almost invariably the χ^2 surface in the space defined by these parameters has many local minima, or valleys, which give fits to the data that are very satisfactory. Thus, in view of the crudeness of the model, it is difficult to determine which one of these minima, if any, has physical meaning.

The variations of the parameters of the optical model as a function of mass number and energy should help us to understand the interaction of various particles with nuclei. Furthermore, the optical model is of value in generating wave functions for elastic scattering, which may then be used in the analysis of nuclear reactions by the distorted-wave Born approximation method. Some element-to-element fluctuations in the parameters are to be expected, particularly since the optical model does not take into account nuclear structure differences and since fitting procedures usually do not make provisions for any possible systematic error in the experimental data.

In this paper we report an optical-model analysis of deuteron elastic scattering from many nuclei for deuteron energies above 10 MeV. Since the deuteron is a very loosely bound structure, one may question whether the optical-model analysis of the elastic scattering can furnish more than a convenient "parametrization" of the data with a potential which has little physical meaning. Hence, several types of analyses are possible, depending on how well one expects the optical model to describe the elastic scattering of deuterons from nuclei. One may look for similarities in the various potentials found by allowing all the parameters of the model to be adjusted for optimum fits to the data as done by Halbert[5]; or, at a sacrifice in the quality of the fits, one may search for a set of parameters which will reasonably fit a large body of data as done by Melkanoff *et al.*[6]

In this analysis an attempt is made to find the dependence of the real and imaginary parts of the potential on mass number and energy. In Sec. II the criteria for analysis of the data and a detailed analysis of the scattering on copper at 11.8 MeV are given. It is found that a series of different potentials can represent the data very accurately. In Sec.III all the data are analyzed with two types of potentials found for copper at 11.8 MeV. In Sec. IV several sets of geometrical parameters are used to analyze the data, allowing only the well depths to be adjusted for a fit, and their dependence on mass number and energy is discussed.

II. PRELIMINARY ANALYSIS

Definition of the Potentials

The optical model used in this analysis is defined by the sum of the following potentials:

real part,

$$-V_S f(r,r_{0S},a_S);$$

imaginary part,

$$-W_S f(r,r_{0I},a_I)+4a_I W_D (d/dr) f(r,r_{0I},a_I).$$

* Consultant.
† Operated by Union Carbide Corporation for the U. S. Atomic Energy Commission.
[1] F. Perey, Phys. Rev. **131**, 745 (1963).
[2] R. N. Maddison, Proc. Phys. Soc. (London) **79**, 264 (1962).
[3] J. S. Nodvik, C. B. Duke, and M. A. Melkanoff, Phys. Rev. **125**, 975 (1962).
[4] R. M. Drisko, University of Pittsburgh (unpublished).
[5] E. C. Halbert, Oak Ridge National Laboratory (to be published).
[6] M. A. Melkanoff, T. Sawada, and N. Cindro, Phys. Letters **2**, 98 (1962).

We also have a Coulomb potential of

$$(Ze^2/2R_C)[3-(r^2/R_C^2)] \quad \text{for } r\leq R_C,$$

and

$$Ze^2/r \quad \text{for } r>R_C.$$

The function $f(r,r_0,a)$ is the usual Woods-Saxon form factor,

$$f(r,r_0,a)=\{1+\exp[(r-r_0A^{1/3})/a]\}^{-1},$$

where A is the atomic mass of the nucleus in atomic mass units.

The imaginary potential is composed of a volume part W_S and a surface part W_D, with the factor $4a_I$ being introduced so that the surface form factor $4a_I(df/dr)$ has unity for its maximum value. The Coulomb potential written would be that produced by a uniform charge distribution of radius R_C. Since the results of the calculation are not sensitive to the value of R_C, during most of the analysis it has been set to the value at which the real part of the potential has fallen to half its maximum value, $R_C=r_{0S}A^{1/3}$.

In addition to the central potential which we considered, a vector spin-orbit potential and various forms of tensor spin-orbit potentials could have been used, since the deuteron has spin 1.[7] However, at the time this analysis was initiated, no results existed on the polarization of deuterons in the elastic scattering from nuclei. Such results have now become available,[8] and a few check calculations have been made to determine the effects of these noncentral spin-orbit potentials. In the case of the vector potential, the effects on the calculated elastic scattering differential cross section are small for the range of elements studied when values of the strength of the vector spin-orbit potential give good agreement with the measured vector polarization[9]; furthermore, they are compensated for by quite small changes in the parameters of the central potential. In the case of the tensor potential, Raynal[10] has reported preliminary calculations for several forms of tensor potentials, and their effects on the parameters reported in this paper are also small. Thus, none of the general conclusions of this analysis should be appreciably affected by our neglect of these noncentral spin-orbit potentials, although they must be included to obtain any vector or tensor polarization.

The program for solving Schroedinger's equation by numerical integration on the IBM-7090 computer at Oak Ridge is the same as used in a previous analysis of proton scattering.[1]

Fitting Criteria Used

The quantitiy χ^2, defined as

$$\chi^2=\frac{1}{N}\sum_{i=1}^{N}\left(\frac{\sigma_{\text{th}}(\theta_i)-\sigma_{\text{exp}}(\theta_i)}{\Delta\sigma_{\text{exp}}(\theta_i)}\right)^2,$$

was selected to compare objectively and quantitatively the fits as a function of the optical potential parameters. Here σ_{th} and σ_{exp} are, respectively, the calculated and experimental values of the cross section at θ_i, and $(\Delta\sigma_{\text{exp}})^{-2}$ is the corresponding weight of σ_{exp}; $\Delta\sigma_{\text{exp}}$ is taken to be the experimental error.

The above expression for χ^2 assumes that the errors are uncorrelated at each data point. However, many of the errors in deuteron elastic scattering results do not come from the statistics of counting and are likely to be correlated in some unknown manner over the angular range of the data. In most cases it would be difficult to take into account properly such correlated errors, even if they are known, and we have for simplicity taken the above criteria for the goodness of fit of the optical model to the data.

When χ^2 is small, of the order of 1, then the calculated curve gives a good description of the data and the exact value of χ^2 is meaningful in conveying the quality of the fit, as subjectively estimated by the eye. However, it often happens that the value of χ^2 is of the order of 10 or more; in such cases, the use of χ^2 alone as a criterion to describe the fit, or lack of it, is not very helpful. If the data as a function of angle show oscillations of large amplitude and the calculated curve is slightly out of phase with them, the value of χ^2 will become large although the general features of the data may still be quite well reproduced. As a result, it is most meaningful to compare the value of χ^2 for a given set of data as a function of the value of the parameters of the model. Also, it will be found that, in general, the value of χ^2 increases with deuteron energy. Since the number and amplitude of the oscillations in the data also increase, the over-all agreement with the data is still acceptable for the highest energies. It should also be noted that the numerical value of χ^2 varies inversely as the square of the assigned experimental errors, which vary from 5 to 15% for the data in this analysis.

The present analysis was made possible by using an automatic parameter-search code in conjunction with the optical-model code. The search code minimizes χ^2 with respect to any desired number of the parameters and permits a detailed study of parameter space. Varying the six parameters of the model, an average time of two minutes is required by the IBM-7090 computer to fit an angular distribution.

TABLE I. Optical-model potentials which fit the 11.8-MeV data for copper.

Set	V_S (MeV)	r_{0S} (F)	a_S (F)	W_D (MeV)	W_S (MeV)	r_{0I} (F)	a_I (F)	σ_R (mb)	χ^2
1	36.8	1.070	0.987	10.07		1.444	0.739	1440	1.4
2	58.5	1.153	0.879	13.32		1.434	0.708	1476	0.65
3	90.7	1.172	0.822	18.34		1.410	0.661	1468	0.78
4	128.2	1.193	0.775	24.3		1.403	0.608	1460	0.84
5	167.8	1.232	0.716	31.9		1.394	0.560	1451	0.96
1′	36.8	1.043	1.006		4.57	2.048	0.443	1502	0.72
2′	61.6	1.122	0.891		6.95	1.891	0.549	1487	0.59
3′	95.5	1.147	0.808		9.57	1.789	0.596	1477	0.67
4′	136.9	1.160	0.753		12.38	1.719	0.612	1472	0.77

[7] G. R. Satchler, Nucl. Phys. **21**, 116 (1960).
[8] R. Beurtey *et al.*, Compt. Rend. **256**, 922 (1963).
[9] G. R. Satchler, Oak Ridge National Laboratory (private communication).
[10] J. Raynal, Phys. Letters **3**, 331 (1963).

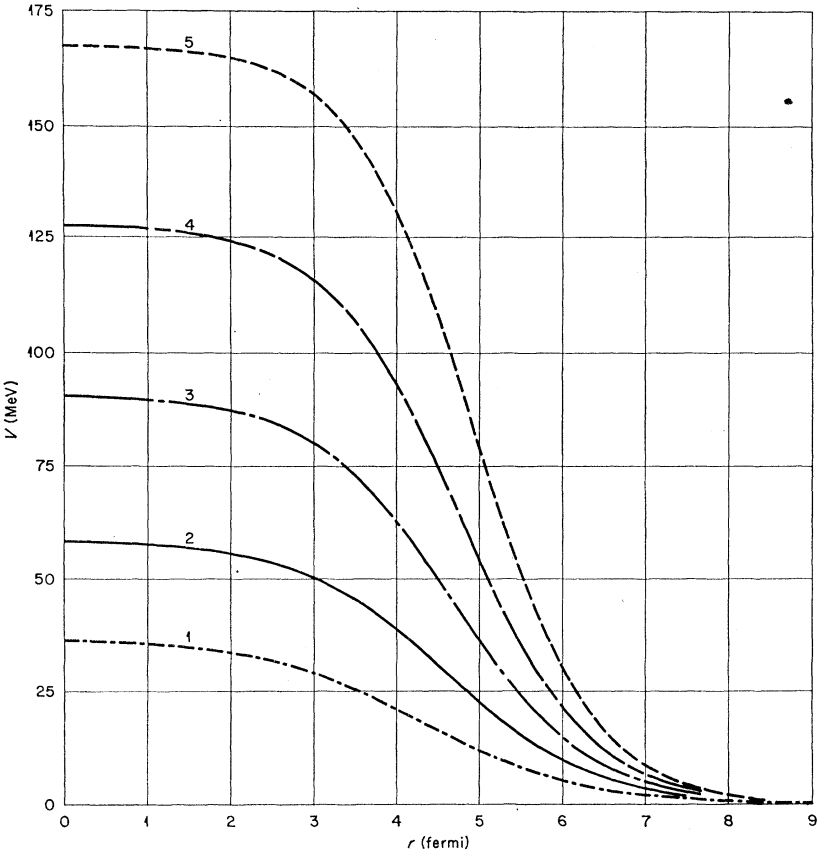

FIG. 1. Real parts of the pure surface absorption potentials which fit the 11.8-MeV data for copper. The parameters of the potentials are given in Table I.

Multiplicity of Potentials

Very early in the analysis many different optical potentials, which gave equally satisfactory fits to the data, were found. For a given potential, it is possible to generate a continuous family of potentials which differ only in that V_S and $R_S(R_S=r_{0S}A^{1/3})$ are varied such that the product $V_S R_S{}^n=$constant. Such invariances are often found in the case of proton and neutron optical-model potentials, but seem to be even more pronounced in the case of deuteron scattering. However, the case of deuterons differs from the other two in that, for a *given value of* R_S, it is possible to find a *discrete set of values of* V_S for which very good fits to the data can be obtained. Although it is possible to find good fits by allowing only the real well depth V_S to change in discrete steps and keeping all other parameters the same, for optimum fits it is better to readjust slightly all the parameters for each value of V_S. It was also found that for optimum fits a discrete value of the imaginary potential is associated with each real well depth. However, equally good fits can be obtained whether the imaginary potential is of the surface type ($W_S=0$) or extends throughout the volume of the nucleus ($W_D=0$).

In Table I is given a series of such potentials which fit the 11.8-MeV data on copper.[11] They are separated according to whether a pure surface or a pure volume imaginary potential is used, the prime denoting the volume imaginary potential. For the case of pure surface absorption, the real parts of the potentials are plotted in Fig. 1. It is clear that the potentials become negligible at the same radius; therefore the same number of partial waves will be required in each case. From Table I it can be noticed that the real parts of the potentials in corresponding cases of surface and volume absorption are not identical but are related by invariances of the type $V_S R_S{}^n=$constant. The imaginary parts of the nine potentials are plotted in Fig. 2. Although the potentials are very different in the interior and at the surface, for $W(r)\lesssim 4$ MeV the tails of all the potentials are very nearly the same.

All the potentials give nearly the same scattering matrix elements S_l, as can be seen in Fig. 3, where some of them are plotted in the S_l plane. Due to the different well depths, the deuteron wave lengths are, of course, always different inside each potential. But a remarkable property of these potentials is that every partial wave, except the highest ones in some cases ($l>8$), has exactly

[11] R. Jahr, K. D. Müller, W. Oswald, U. Schmidt-Rohr, Z. Physik **161**, 509 (1961); G. Igo, W. Lorenz, and U. Schmidt-Rohr, Phys. Rev. **124**, 832 (1961).

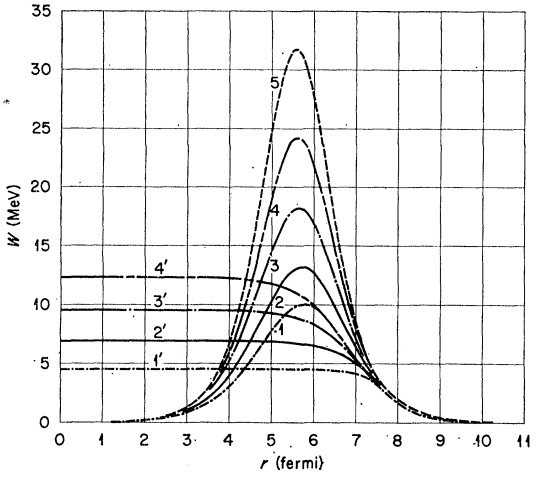

FIG. 2. Imaginary parts of the optical-model potentials which fit the 11.8-MeV data for copper. The parameters of the potentials are given in Table I.

one more half-wavelength inside the well than the corresponding partial wave in the next shallower well. This is shown for two partial waves in Fig. 4, where the moduli of the partial waves are plotted as a function of radius for the five surface-absorption potentials. Note that, as implied by the equality of all the scattering matrix elements, all the radial wave functions are the same just outside the potential. The total wave functions in each case are different in the interior region of the potential. This is shown in Figs. 5 and 6, where the moduli of the wave functions for the nine potentials are plotted along the axis of the beam.

The multiplicity of the potentials for deuteron scattering has been verified for other elements at 11.8 MeV, as well as at 21.6 MeV, and appears to be characteristic of the optical-model treatment of deuteron elastic

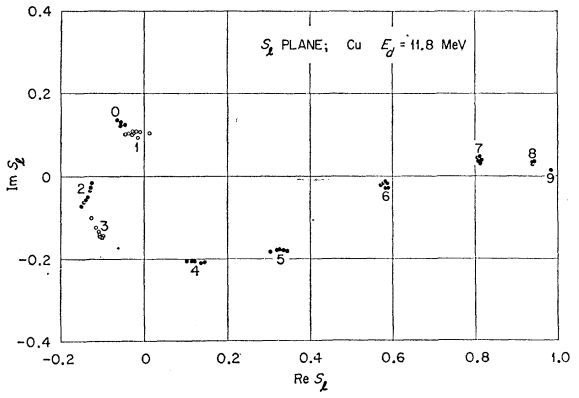

FIG. 3. Distribution of scattering matrix elements, S_l, from all the optical model fits to the 11.8-MeV data for copper. The parameters of the potentials are given in Table I. The number associated with each cluster of points indicates the partial wave to which the scattering matrix elements correspond. For clarity, not all the points have been shown, but the size of the cluster indicates the spread of the values.

scattering. This behavior is also found in alpha particle scattering[12] and may be associated with the fact that we are dealing with strongly absorbed particles.

The deuteron being a weakly bound unit, it has been suggested[13] that the Coulomb breakup and the polarizability of the deuteron are important in the scattering of deuterons from nuclei. However, all the potentials found in fitting the data do not display the large tails which one would associate with such an effect if it were dominant. It may be rather significant that the tails of all the imaginary potentials are similar in the surface of the nucleus, where the real part of the potential for neutron and proton scattering is a few MeV deep. As a naive interpretation, this potential of a few MeV should be sufficient to break up the deuteron. It would then

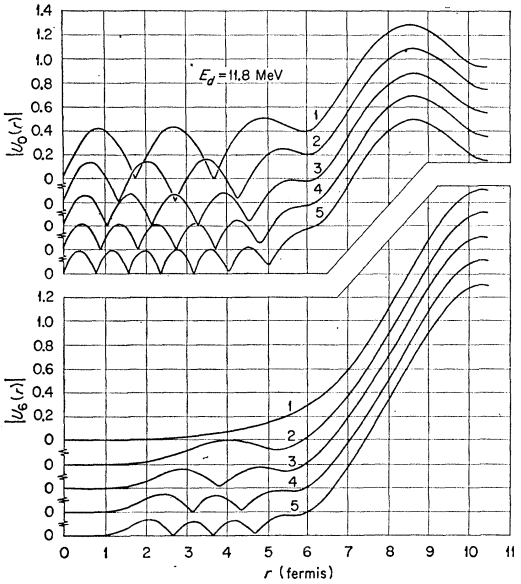

FIG. 4. Moduli of the $l=0$ and $l=6$ partial waves as a function of radius for the pure surface absorption potentials which fit the 11.8-MeV data for copper. The parameters of the potentials are given in Table I. The potentials which generated the wave functions are shown in Figs. 1 and 2.

seem that the dominant physical phenomenon is the breakup of the deuteron as it penetrates the nuclear surface and not the breakup or the polarizability of the deuteron in the Coulomb field of the nucleus, at least in the domain of energies considered in this analysis.

On the basis of elastic scattering alone, there does not appear to be a way to distinguish between the different potentials. Analysis of the inelastic scattering of deuterons, where collective states of the nucleus are excited, may help in differentiating between the various potentials. However, if the calculation is sensitive only to the wave functions at the surface of the nucleus, one

[12] R. M. Drisko, G. R. Satchler, and R. H. Bassel, Phys. Letters **5**, 347 (1963).

[13] C. F. Clement, Phys. Rev. **128**, 2728 (1962); see this paper for earlier references on Coulomb breakup of the deuteron.

may still obtain the same results for the different potentials. The analysis of stripping reactions in the distorted-wave Born approximation is more sensitive to the part of the wave function inside the nucleus, but in view of the fact that the deuteron is very weakly bound, it is even more difficult to believe that the wave function inside the nucleus is correct than it is to believe in the correctness of the wave function in the surface region. In order to provide optical potentials which may be useful in distorted-wave Born approximation calculations, it was decided to do a systematic analysis of most

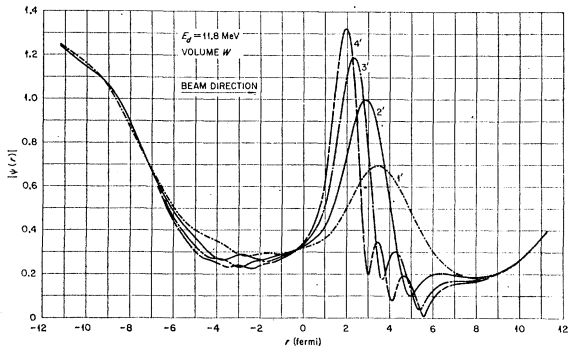

FIG. 5. Moduli of total wave functions of the pure volume absorption potentials plotted along the axis of the beam for copper at 11.8 MeV. The parameters of the potentials are given in Table I.

of the available deuteron elastic scattering data using two of the types of potentials previously found. The two families selected correspond to the ones called 2 and 3 in Fig. 1; in the remaining part of this analysis they will be referred to as a and b, respectively. The potential a is the one which has a real well depth that most closely resembles the neutron and proton potential. The potential b has a well depth which is nearly the sum of the neutron and proton well depths, which in a naive interpretation should be close to the potential seen by the deuteron.

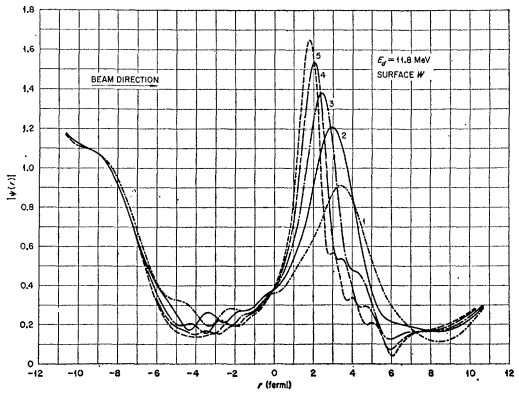

FIG. 6. Moduli of total wave functions of the pure surface absorption potentials plotted along the axis of the beam for copper at 11.8 MeV. The parameters of the potentials are given in Table I.

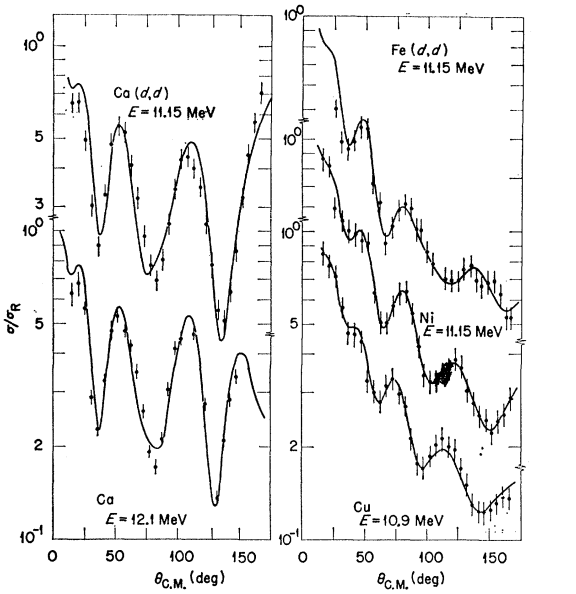

FIG. 7. Comparison of the data at 10.9, 11.15, and 12.1 MeV with the curves from the set a parameters given in Appendix I. All the parameters of the potentials were adjusted by the code for a minimum χ^2.

III. "BEST FITS" TO THE DATA FOR SETS a AND b

Selection of the Data

Although a large body of experimental data on the elastic scattering of deuterons from nuclei is available, only a fraction of it was used for this analysis. Data on the scattering from the very light nuclei were not analyzed for two reasons: first, large fluctuations in the optical-model parameters are expected from structure effects and possibly from insufficient energy-averaging of the data; and second, the effects on the angular distribution of the spin-orbit potential, which we have neglected, is more important for light nuclei[9] than for heavy nuclei. Since the systematic optical-model analysis of neutron[14] and proton[1] elastic scattering data does seem to be successful for nuclei as light as $Z=13$, however, with potentials that vary smoothly as a function of A, we have tried to include the data for nuclei with $Z\geq 12$. But we found that when the data do not show much of a diffraction pattern, it is particularly difficult to find an unambiguous set of optical-model parameters. We have, therefore, found it preferable to analyze only the data for deuteron energies above 10 MeV. Since one aim of this analysis was to determine the behavior of the optical-model parameters as a function of both mass number and energy, we then restricted ourselves to a few energies above 10 MeV, where scattering from a large number of nuclei had been studied experimentally. Even with these restrictions we were left with 52 angular distributions to analyze in the range of 11 to 22 MeV, with particular emphasis on data at 11.8, 15.0 and 21.6 MeV. A sum-

[14] F. Perey and B. Buck, Nucl. Phys. **32**, 353 (1962).

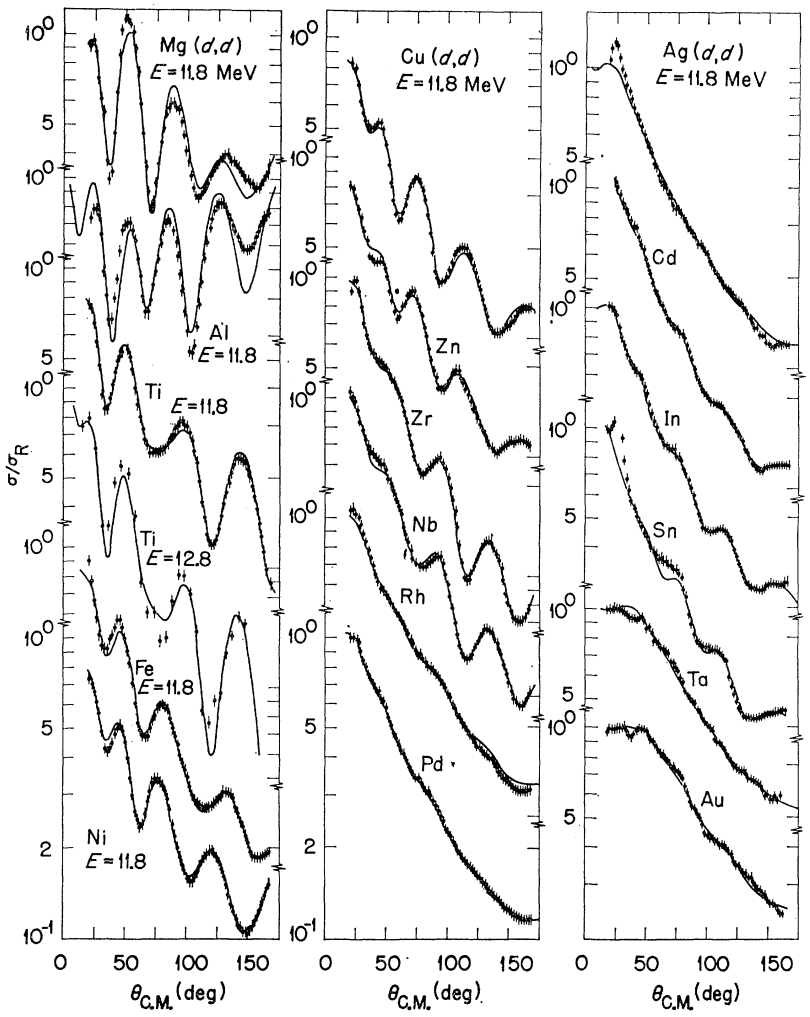

FIG. 8. Comparison of the data at 11.8 MeV for several elements and the data at 12.8 MeV for titanium with the curves from the set a parameters given in Appendix I. All the parameters of the potentials were adjusted by the code for a minimum χ^2.

TABLE II. Sources of experimental data.

Energy (MeV)	Investigator(s)	Estimated errors
10.9	Takeda[a]	±9%
11.15	Takeda[a]	±9%
11.8	Jahr *et al.*[b]	5%
12.1	Strzalkowski[c]	10%,5%
12.8	Strzalkowski[c]	6%,5%
13.5	Cindro and Wall[d]	5%[e]
15.0	Cindro and Wall[d]	5%[e]
	Jolly *et al.*[f,g]	10%[h]
18.1	Ishizaki *et al.*[i]	5%
~21.5	Yntema[j]	5%
27.5	Mayo[k]	10%,20%

[a] See Ref. 15.
[b] See Ref. 11.
[c] See Ref. 16.
[d] See Ref. 17.
[e] 10% at very small and very large angles.
[f] See Ref. 18.
[g] Distinguished from Cindro and Wall data by an asterisk.
[h] 15% at very large angles.
[i] See Ref. 19.
[j] See Ref. 20.
[k] See Ref. 21.

mary of the sources of data, along with the errors estimated by the experimentalists for each set, is given in Table II.

Results for Sets a and b

Each of the 52 angular distributions was fitted for both set a and set b by the search code by allowing the six optical-model parameters to be simultaneously adjusted for a least-square fit to the data. The starting values of the parameters bias the search code to find a minimum in χ^2 space corresponding to potentials of type a or b. The parameters which were so obtained are given in Appendix I. In a few cases, the radius parameters, real or imaginary, had very small values and had

[15] M. Takeda, J. Phys. Soc. Japan **15**, 557 (1960).
[16] A. Strzalkowski, Phys. Letters **2**, 121 (1962).
[17] N. Cindro and N. S. Wall, Phys. Rev. **119**, 1340 (1960).
[18] R. K. Jolly, E. K. Lin, and B. L. Cohen, Phys. Rev. **130**, 2391 (1963).
[19] Y. Ishizaki, Y. Saji, T. Ishimatsu, T. Nakamura, Y. Nakano, and S. Yasumi, Institute for Nuclear Study, University of Tokyo, Japan, Report No. INSJ-44 (unpublished).
[20] J. L. Yntema, Phys. Rev. **113**, 261 (1959).
[21] S. Mayo (private communication to G. R. Satchler).

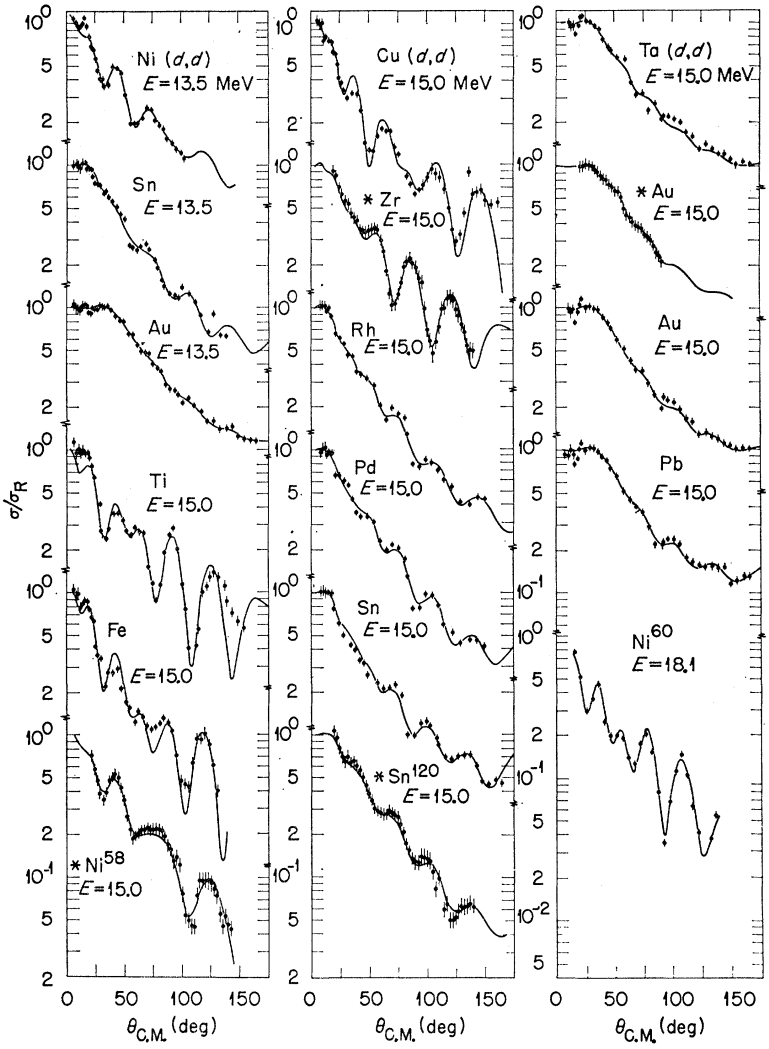

FIG. 9. Comparison of the data at 13.5, 15.0, and 18.1 MeV with the curves from the set a parameters given in Appendix I. All the parameters of the potentials were adjusted by the code for a minimum χ^2.

to be kept fixed at the values indicated in Appendix I in order to obtain a fit to the data with "reasonable" radius parameters. The data and the curves corresponding to the parameters of set a are shown in Figs. 7–10. Although not shown in the figures, the curves corresponding to the parameters of set b are very similar to those of set a, as can be inferred from the values of χ^2 for the two types of potentials in Appendix I. In general, the data are fitted very well with the exception of the lightest elements studied, i.e., aluminum, magnesium, and calcium. We continued to analyze these light elements, but we attach very little weight to the values of their parameters.

Nearly all the parameters of both sets vary by a factor of almost 2. However, for each angular distribution, the trends observed in Table I are apparent in Appendix I. That is, in 75% of the cases $r_{0S}(a)<r_{0S}(b)$; in 87% of the cases $a_S(a)<a_S(b)$; for the imaginary part of the potential $W_D(a)<W_D(b)$ for all the elements; in 89% of the cases $r_{0I}(a)>r_{0I}(b)$; and in 85% of the cases $a_I(a)>a_I(b)$. For the values of χ^2, in 85% of the angular distributions $\chi^2(a)\leq\chi^2(b)$, but in only 40% of the cases is χ^2 improved by more than 20%.

Plots of V_S and a_S as a function of r_{0S} are given in Fig. 11 for all the data and for both set a and set b. An invariance of the type $V_S r_{0S}{}^n=$constant is clearly apparent for both types of potential, but the spread of the points is greater for set a than for set b. The plots of a_S versus r_{0S} also reveal some trends. In general, a_S decreases when r_{0S} increases. There is clearly no preferred radius parameter between the limit of about 1.0 to 1.4 F, although it is evident that the radii tend to be smaller for set a than for set b.

For the imaginary parts of the potentials, the diffuseness parameters a_I have less scatter than do the parameters a_S, most of the values being around (0.7 ± 0.1) F for set a and around (0.65 ± 0.1) F for set b. The imaginary radius parameters r_{0I} also have less of a spread in value, being approximately uniformly distributed between 1.2 and 1.5 F. However, it may be more

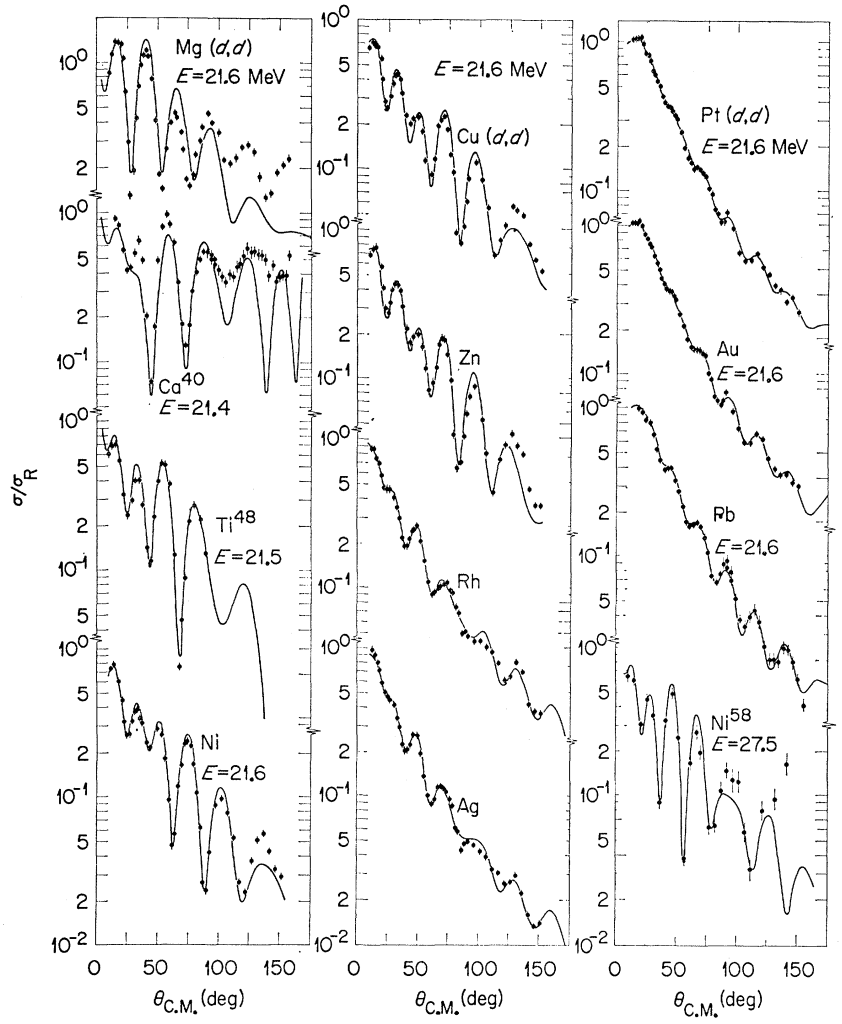

FIG. 10. Comparison of the data at 21.6 and 27.5 MeV with the curves from the set a parameters given in Appendix I. All the parameters of the potentials were adjusted by the code for a minimum χ^2.

significant to compare the tails of the imaginary potentials. The values of the integral

$$I=\int_{R_1}^{\infty} W_D(r)dr,$$

where R_1 is some arbitrary radius in the surface of the nucleus, are a rough measure of the tails of the potential. With $R_1=(1.25A^{1/3}+1.5)$ F, 70% of the potentials give a value of 7.75 ± 1.5 for set a and 65% of the potentials give a value of 8.75 ± 1.7 for set b.

Other features of the parameters are discussed in detail by Halbert,[5] who has performed an independent analysis of deuteron elastic scattering on a smaller set of data. Her analysis differs in that she allows all the parameters of the optical potential to be varied.

IV. ANALYSIS OF THE DATA WITH THE SAME GEOMETRICAL PARAMETERS

Because of the large spread in the optical-model parameters discussed in Sec. III, we selected a series of angular distributions from medium-weight nuclei and analyzed them further in an attempt to determine "average" sets of geometrical parameters. Medium-weight nuclei were chosen because of the lack of success in analyzing the results for light nuclei and because the angular distributions for the heavy elements do not have pronounced diffraction patterns. In the discussion below we will first indicate the procedure used to determine the average geometrical parameters and then give the results of the analysis of all the angular distributions using these parameters and allowing only the well depths to be adjusted for a best fit to the data.

Determination of "Average" Geometrical Parameters

At 11.8 MeV the average value of the radius parameter r_{0S} in Appendix I for the medium-weight elements Fe, Ni, Cu, Zn, Zr, Nb, and Cd is 1.14 F for set a and 1.18 F for set b. If one sets r_{0S} equal to these average values and fits the data for a minimum χ^2 allowing all

TABLE III. "Average" sets of geometrical parameters of the potentials used to analyze the data.[a]

Set	$r_{0S}=r_{0C}$ (F)	a_S (F)	r_{0I} (F)	a_I (F)
A	1.15	0.87±0.06	1.37±0.05	0.70±0.05
B	1.15	0.81±0.04	1.34±0.05	0.68±0.07
C	1.30	0.79±0.05	1.37±0.05	0.67±0.03
D	1.30	0.73±0.04	1.34±0.06	0.65±0.04

[a] The errors shown are the maximum deviations of the individual values from the average.

the other parameters to be readjusted by the code, χ^2 for each element is not increased by more than a few percent. In fact, r_{0S} can be set equal to 1.15 F for both types of potentials without χ^2 increasing by more than a few percent. Furthermore, if one also fixes W_D at around 15 MeV for set a and 20 MeV for set b, the spread in the geometrical parameters a_S, r_{0I}, and a_I is very much reduced and χ^2 does not increase by more than 20%.

It was, therefore, decided to use the angular distributions for Fe, Ni, Cu, Zn, and Cd at 11.8 MeV, for Ni at 18.1 MeV, and for Ni, Cu, and Zn at 21.6 MeV to determine the average geometrical parameters. With $r_{0S}=1.15$ F for both types of potentials and with $W_D=15$ MeV for type a and 20 MeV for type b, the data were refitted allowing only V_S, a_S, r_{0I}, and a_I to be adjusted by the code for the lowest χ^2 on each angular distribution. The average values of the parameters so obtained are given in Table III, in which the maximum deviations from the average values are also indicated. The set of geometrical parameters labeled A corresponds to potentials of type a and the one labeled B to the type b potentials. Since the two sets of parameters are very similar, we attempted to use only one set of parameters, $r_{0S}=1.15$ F, $a_S=0.84$ F, $r_{0I}=1.35$ F, and $a_I=0.69$ F, for both types of potentials; however, the fits thus obtained were worse at 11.8 MeV than when separate parameter sets were used, so we kept the two different geometries A and B. The crosses labeled A and B on Fig. 11 indicate the position of the average parameters for the real part of the potentials.

One of the striking features of parameter sets A and B is the small radius parameter r_{0S}. Neutron and proton optical-model analyses in the same energy range give values around 1.25 F. In view of the large size associated with the deuteron, one would have expected a slightly larger radius parameter for the deuteron optical-model potential. It was, therefore, decided to try to use a radius parameter $r_{0S}=1.30$ F. The same set of elements and the same procedure indicated above were used to determine a new set of average parameters with a real radius parameter of 1.30 F. The results are given in Table III. The geometry labeled C corresponds to potentials of type a and the one labeled D to those of type b. The crosses labeled C and D on Fig. 11 indicate the new average parameters for the real part of the potentials.

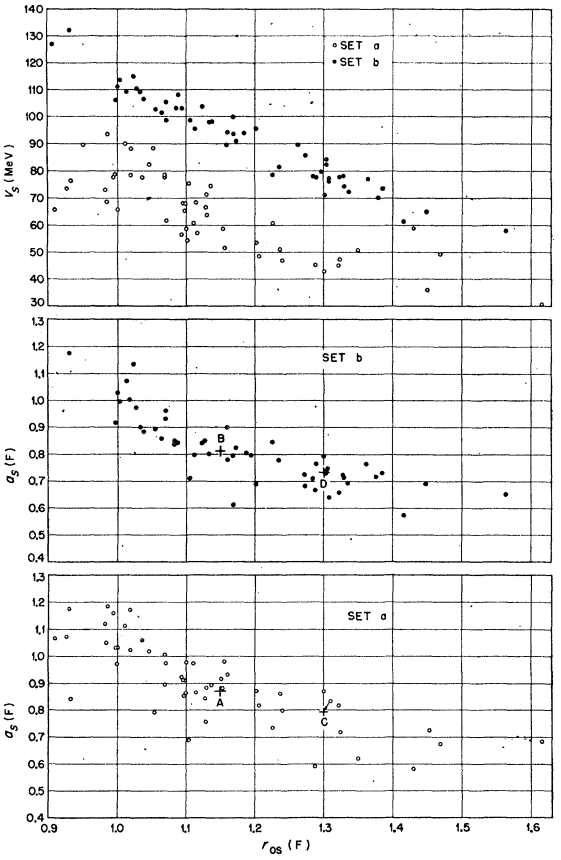

FIG. 11. Well depths and diffuseness parameters of the real part of the potential as a function of the real radius parameter for the sets a and b. The numerical values of the parameters are given in Appendix I. The crosses indicate the values of the real potential geometrical parameters used in Sec. IV to analyze all the data.

Results for Parameter Sets A, B, C, and D

The 52 angular distributions were fitted for each set of geometrical parameters by allowing the search code to adjust V_S and W_D for the lowest χ^2 for each angular distribution. The resulting values for V_S, W_D, the reaction cross section σ_R, and χ^2 are given in Appendixes II–V for the parameter sets A, B, C, and D, respectively. The data and the angular distributions for parameter set C are given in Figs. 12–15. In general, the fits for the other parameter sets are very similar to the fit for parameter set C; that is, when an angular distribution in a particular range of angles is not well fitted by parameter set C, it usually is not well fitted by the other parameter sets. To illustrate this point, all the fits for copper at 11.8 and 21.6 MeV are given in Fig. 16, along with the angular distributions obtained with the parameters of Melkanoff *et al.*[6]

In Fig. 17, the real potential well depths at the three bombarding energies 11.8, 15.0, and 21.6 MeV are plotted as a function of the Coulomb parameter $Z/A^{1/3}$. The lines on Fig. 17 are drawn to indicate the trends of V_S as a function of $Z/A^{1/3}$; the slopes were determined

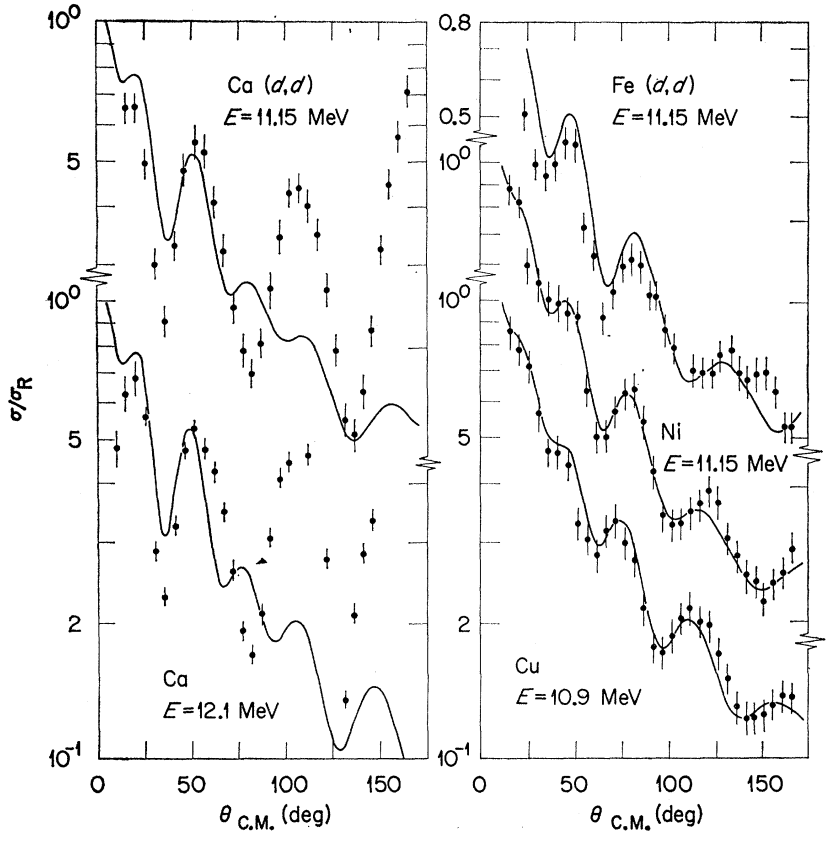

FIG. 12. Comparison of the data at 10.9, 11.15, and 12.1 MeV with the curves from the set C parameters. The geometrical parameters are kept fixed to the values given in Table III and the well depths, V_S and W_D, given in Appendix IV, are adjusted for the lowest χ^2.

from the 15.0- and 21.6-MeV points, and the same slope is used for the 11.8-MeV data in each case.

In Fig. 18, the imaginary potential well depths at the three bombarding energies 11.8, 15.0, and 21.6 MeV are plotted as a function of $A^{1/3}$. Owing to the large fluctuations, no average line is drawn, but the trends will be commented upon later.

The energy dependences of the real well depths for nickel are shown in Fig. 19 for the four different geometries, as well as the relative position of the lines of Fig. 17. The energy dependences of the imaginary potential well depths W_D for titanium, nickel, and copper are shown in Fig. 20 for the four different geometries.

Remarks on the Results for Fixed Geometries

Real Part of the Potential

In Fig. 17 it is evident that the relative values of the well depths are, in general, independent of the set of geometrical parameters used. Also, the well depths for nickel, copper, and zinc all have the same relative values at 11.8 and 21.6 MeV. At 11.8 MeV the fits for the light nuclei are not very good, and the real well depths do not follow the trend of the other nuclei as a function of $Z/A^{1/3}$. Also at 11.8 MeV, the well depths for tantalum and gold are too high, but the lack of structure in the angular distributions may be partially responsible for this. In the case of sets A and B, the real well depth for tantalum was fixed at the value shown because of the tendency for the search code to obtain the next deepest solution. At 21.6 MeV, the linear trend of V_S as a function of $Z/A^{1/3}$ is very clearly shown for the four sets of geometrical parameters. At 15.0 MeV this is also true, but for nickel the values are consistently too low and for rhodium and palladium the values are too high.

The dependence of V_S on $Z/A^{1/3}$ is smaller for the deeper potentials and decreases when the radius parameter r_{0S} is increased. If these trends continue, there should not be any $Z/A^{1/3}$ dependence of V_S for a sufficiently large radius parameter r_{0S}. An investigation was made to find an upper limit to r_{0S}. Using the same group of angular distributions and the same method as before, but with $r_{0S}=1.50$ F, we obtained the following sets of average parameters expressed in fermis:

Set E: $r_{0S}=1.50$, $a_S=0.67\pm0.04$;
$r_{0I}=1.41\pm0.08$, $a_I=0.60\pm0.04$;
Set F: $r_{0S}=1.50$, $a_S=0.61\pm0.04$;
$r_{0I}=1.40\pm0.06$, $a_I=0.55\pm0.09$.

For set E the well depths were around 35 MeV and for set F about 60 MeV. These two sets of parameters were

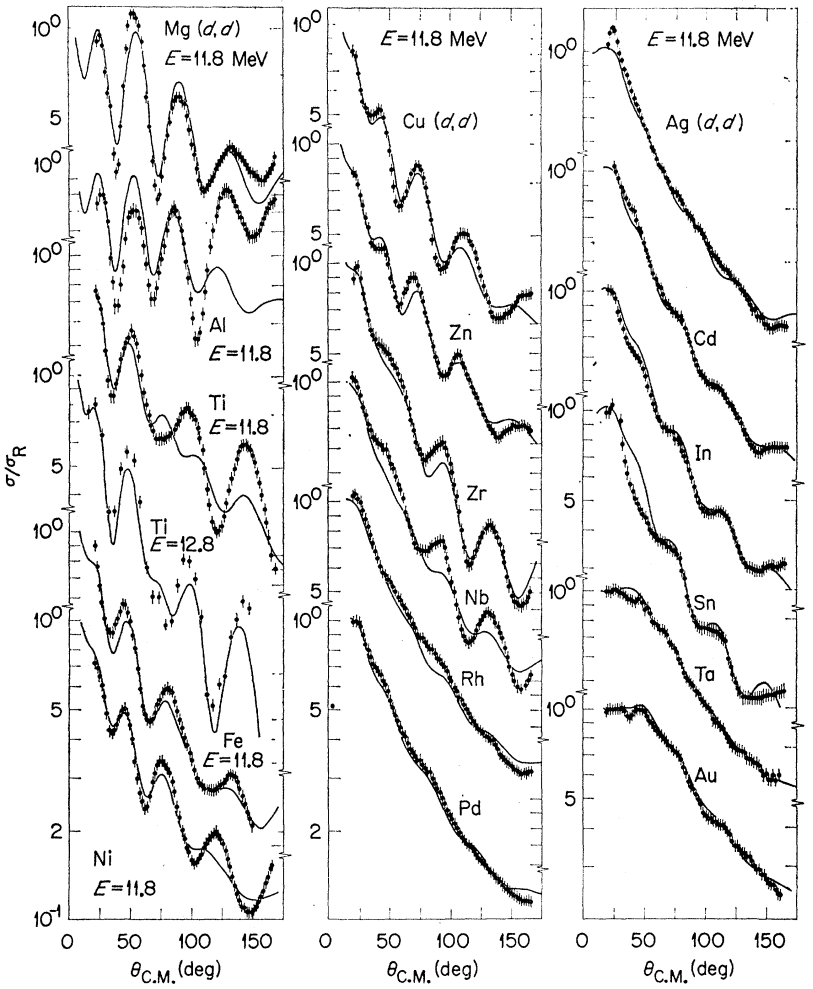

FIG. 13. Comparison of the data at 11.8 MeV for several elements and the data at 12.8 MeV for titanium with the curves from the set C parameters. The geometrical parameters are kept fixed to the values given in Table III and the well depths, V_S and W_D, given in Appendix IV, are adjusted for the lowest χ^2.

not investigated in detail because the minimum χ^2 values obtained when all the parameters were allowed to vary (except r_{0S}, fixed at 1.50 F) were two to three times higher than they were under similar conditions when r_{0S} was either 1.15 or 1.30 F. This indicates that $r_{0S}=1.50$ F is close to an upper limit for an acceptable radius parameter.

The type of potential used by Melkanoff *et al.*[6] corresponds to set F, but they used only a complex Woods-Saxon potential. However, this does not seem to be a large restriction in their case, since for sets E and F the real and imaginary radius parameters are very similar and the values of a_S and a_I are also nearly equal. If it is the tail of the imaginary part of the potential which is important, the fact that we use a different form factor for the imaginary part of the potential is not very significant, because in the external region the shape of the derivative Woods-Saxon potential is very similar to the shape of a Saxon potential having the same diffuseness parameter. Melkanoff *et al.*[6] found that they did not need a $Z/A^{1/3}$ dependence of V_S, which is in agreement with the trends mentioned above.

In Fig. 19 it is easy to draw a linear energy dependence for V_S in the case of sets A, B, and C. The line drawn for set D does not take into account the value of V_S at 27.5 MeV; if more weight were attached to this point, it is possible that the slope of the line could be as low as the one for set B, but there would be considerably more scatter of the points than for the other sets. In any case, the energy dependence is smaller the deeper the well; in going from set A to set B it is reduced by a factor of 2. This could also be the case for sets C and D.

The analysis of the deuteron elastic scattering data

TABLE IV. Parameters of the potentials obtained from the systematic analysis.[a]

Set	$r_{0S}=r_{0C}$ (F)	a_S (F)	r_{0I} (F)	a_I (F)	V_{0S} (MeV)	K_1	K_2
A	1.15	0.87	1.37	0.70	42	3.3	0.51
B	1.15	0.81	1.34	0.68	81	2.0	0.22
C	1.30	0.79	1.37	0.67	37	2.4	0.51
D	1.30	0.73	1.34	0.65	75	1.14	0.42

[a] The coefficients V_{0S}, K_1, and K_2 refer to formula (1) in the text.

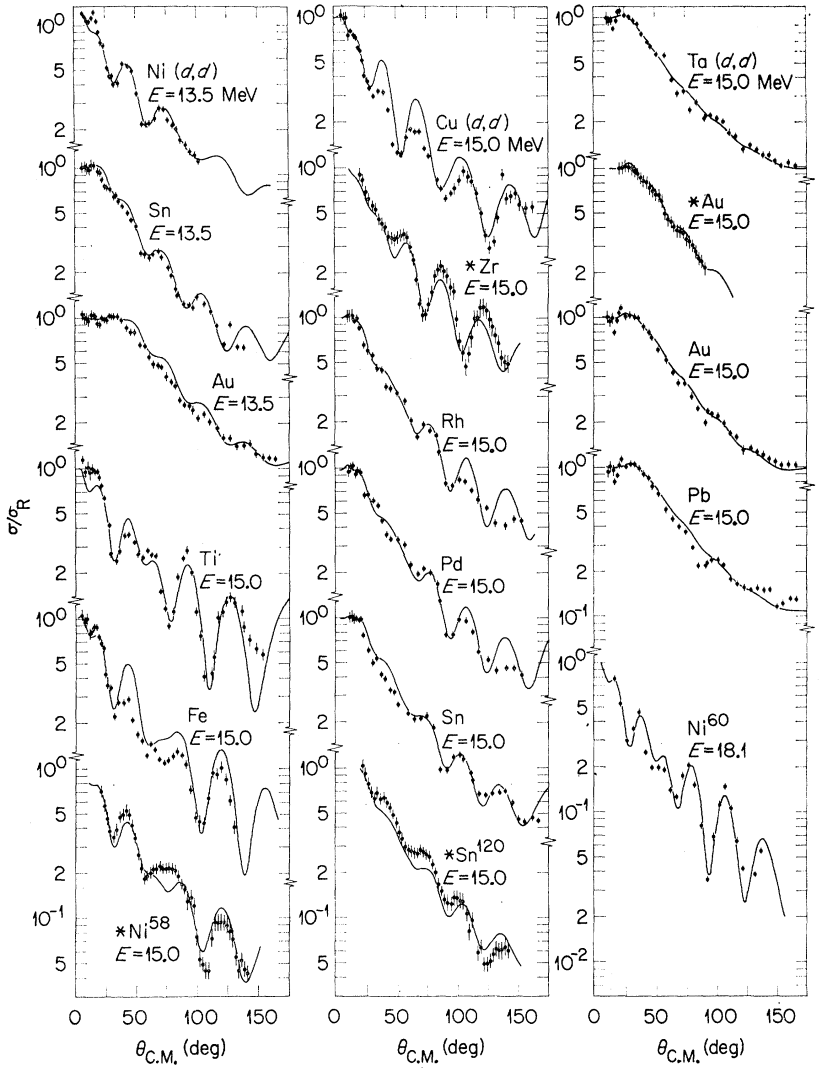

FIG. 14. Comparison of the data at 13.5, 15.0, and 18.1 MeV with the curves from the set C parameters. The geometrical parameters are kept fixed to the values given in Table III and the well depths, V_S and W_D, given in Appendix IV, are adjusted for the lowest χ^2.

shows that the real well depths can be represented by the following empirical formula:

$$V_S = V_{0S} + K_1(Z/A^{1/3}) - K_2E, \quad (1)$$

the values of V_{0S}, K_1, and K_2 being given in Table IV for the four sets of geometrical parameters studied. A similar dependence on energy and $Z/A^{1/3}$ is observed in the scattering of protons from nuclei,[1] but in the case of protons, the dependence can be explained in terms of the isotopic spin dependence of the nuclear forces and the momentum dependence of the potential.

It was shown in Ref. 1 that, due to the momentum dependence of the real well depth, an approximate relationship between the parameters K_1 and K_2 is

$$K_1 = 1.38K_2.$$

This does not seem to hold for the potentials we have studied. Since the coefficient K_1 decreases as r_{0S} is increased, it would seem that the above relation could hold at around $r_{0S} = 1.5$ F. But we have already pointed out that according to our analysis such large radii give fits to the data which are somewhat worse than for lower values of r_{0S}.

Imaginary Part of the Potential

Comparison of the four sets of geometrical parameters studied plus those of sets E and F shows that, to a large degree, the invariance of the type $V_S R_{0S}^n = \text{constant}$, which they represent, has only a small effect on the parameters of the imaginary part of the potential.

In Fig. 18, only set B gives a clear indication of a trend of W_D as a function of mass number, the trend being a systematic decrease at all three energies. Here again, as was the case for the real well depth V_S, the relative values of W_D are approximately the same for all the four average geometries used despite the large fluctuations. It is also evident that for nearly all nuclei W_D is smaller at 15 MeV than at 21.6 MeV or at 11.8

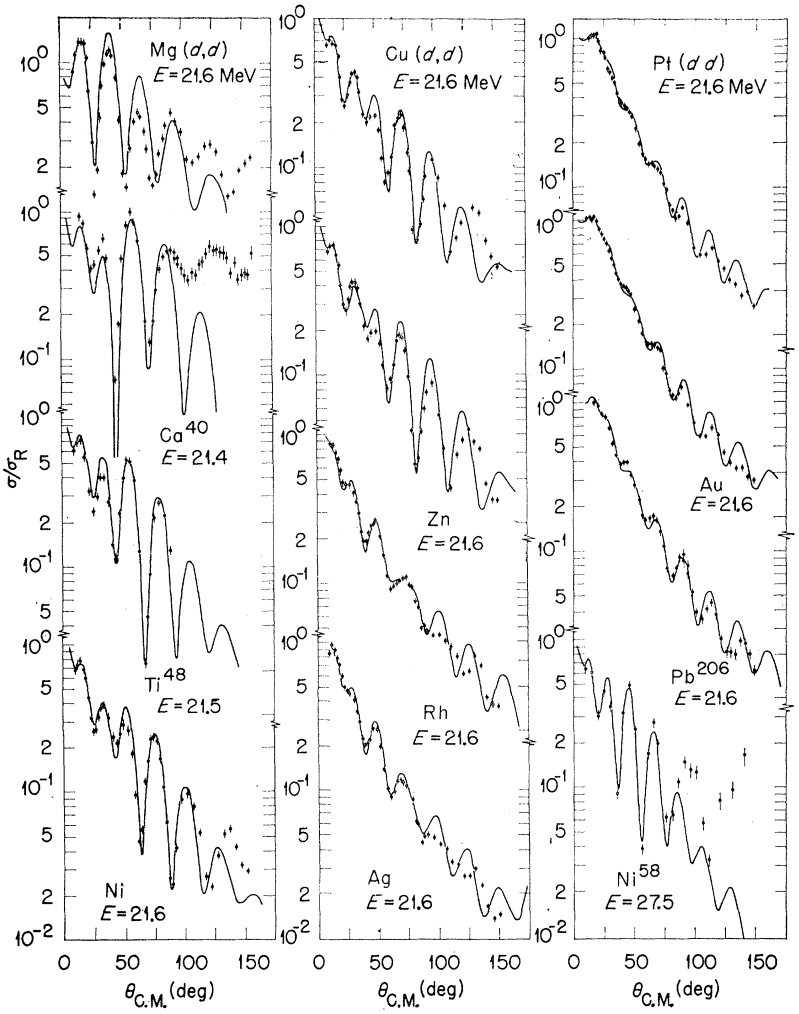

FIG. 15. Comparison of the data at 21.6 and 27.5 MeV with the curves from the set C parameters. The geometrical parameters are kept fixed to the values given in Table III and the well depths, V_S and W_D, given in Appendix IV, are adjusted for the lowest χ^2.

MeV. This very peculiar phenomenon is clearly shown in Fig. 20, where the energy dependence of W_D for the medium-weight nuclei titanium, nickel, and copper is given. Above 15 MeV for all the geometries one may represent the increase in W_D for medium-weight nuclei by

$$W_D = W_{0D} + 0.24E.$$

But between about 11 and 14 MeV the value of W_D decreases by approximately 6 MeV for the four sets. This sudden change in the energy dependence of W_D, if real (that is, if not associated simply with the method of analysis), may indicate that 15 MeV is a transition energy for medium-weight nuclei with a different physical mechanism dominating the deuteron elastic scattering above and below this energy. One could imagine that at lower energies Coulomb breakup should dominate but that as one goes above the Coulomb barrier the breakup of the deuteron in the nuclear field could become more important. We should observe a strong Z dependence of W_D at a given bombarding energy if the above explanation were valid and reflected in the optical-model analysis by first a rapid decrease of W_D as a function of energy followed by a slow increase of W_D. This is not the case; in fact, the only Z dependence observed is for set B and it is contrary to the interpretation given above. Since one normally expects a slow increase of W_D as a function of energy, this leaves the energy dependence of W_D below 15 MeV unexplained and renders difficult the extrapolation of the parameters of this analysis to lower energies.

In Fig. 21 are shown the data[22] on nickel at 4.07 MeV and the results of three calculations. The full curve was obtained by using the geometrical parameters of set C and formula (1) to determine the real well depth of $V_S = 52$ MeV. The value of W_D was set at the average value of 16 MeV for set C in Fig. 20, ignoring the rise in W at lower energy. The dashed curve is a fit obtained by the search code using the set C geometrical parameters but allowing the code to adjust V_S and W_D for a best fit. Values of $V_S = 129$ MeV and

[22] I. Slaus and W. P. Alford, Phys. Rev. **114**, 1054 (1959).

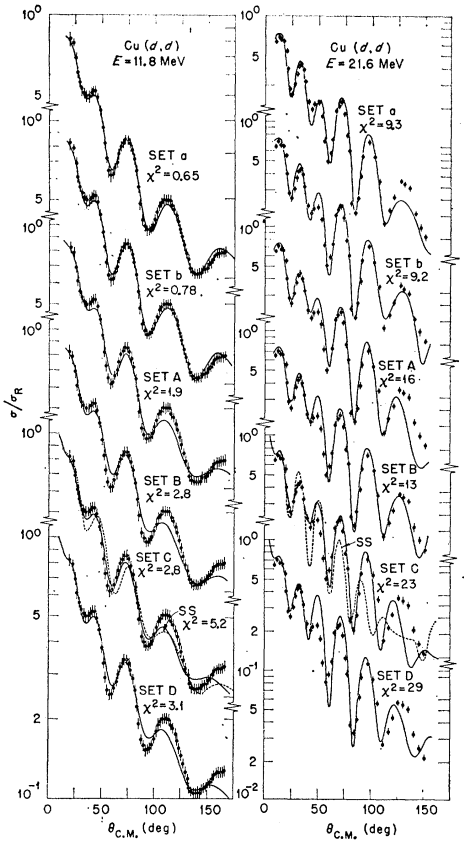

FIG. 16. Comparison of the data at 11.8 and 21.6 MeV for copper with the curves from all the types of potentials. Sets a and b are obtained by allowing all six parameters of the model to be adjusted for the lowest χ^2. For sets A, B, C, and D only the well depths V_S and W_D are adjusted by the code for a best fit, the geometrical parameters of the potentials being kept fixed at the values given in Table III. Note the great similarity between the curves for sets A, B, C, and D. The dashed curves labeled *SS* were obtained from the parameters of Melkanoff *et al.* (see Ref. 6).

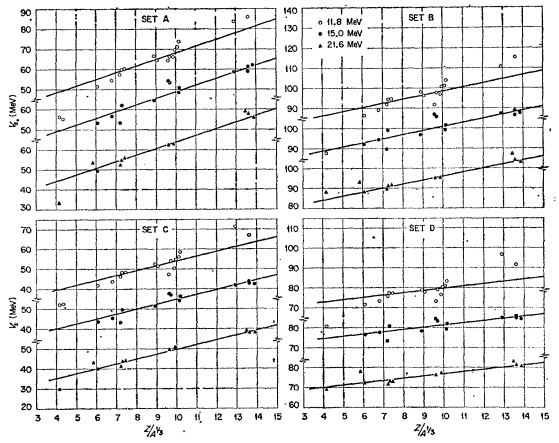

FIG. 17. Real potential well depths, V_S, as a function of the Coulomb parameter $Z/A^{1/3}$ for the fits to the 11.8-, 15.0-, and 21.6-MeV data. The potentials were obtained by adjusting the two well depths, V_S and W_D, for the lowest χ^2 when the geometrical parameters were fixed to the values given in Table III. The numerical values of the well depths are given in Appendixes II–V.

$W_D=72.5$ MeV were obtained. The dotted curve was calculated by using the parameters of Melkanoff *et al.*,[6] which in our notation are $V_S=60$ MeV, $r_{0S}=1.50$ F, $a_S=0.68$ F, $W_S=15$ MeV, $r_{0I}=1.50$ F, and $a_I=0.68$ F. As can be seen from the large differences in the parameters and the small differences in the calculated curves, it is difficult to determine with confidence the trends of the parameters toward lower energies. Data for medium-weight nuclei at closely spaced energies between 4 and 12 MeV would be needed to determine the behavior of W_D at low energies.

Reaction Cross Sections

The various optical-model parameters found in this analysis predict reaction cross sections, σ_R, which are very similar. The six different sets of parameters given in the appendix for all the data analyzed give values of

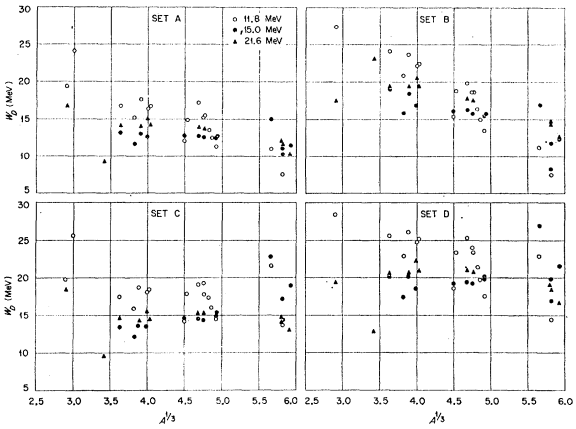

FIG. 18. Surface imaginary potentials, W_D, as a function of $A^{1/3}$ for the fits to the 11.8-, 15.0-, and 21.6-MeV data. The potentials were obtained by adjusting the two well depths, V_S and W_D, for the lowest χ^2 when the geometrical parameters were fixed to the values given in Table III. The numerical values of the well depths are given in Appendixes II–V.

σ_R which differ in general by not more than 5%, and only in a few cases by as much as 10%. Recently, some total reaction cross sections have been measured at 22.4 MeV by Wilkins and Igo.[23] Their results are plotted in Fig. 22, together with the σ_R obtained from the analysis of the 21.6-MeV data with the parameters of set C. The predicted cross sections follow the trend of the data very well but are systematically too high by about 10%. At 12.8 MeV the measured reaction cross sections on Ni^{60} and Ni^{58} were found[24] to be 1523 ± 120 mb and 1588 ± 125 mb, respectively. The average values of σ_R for the six different potentials fitting the data on natural nickel are 1408 mb at 11.8 MeV and 1472 mb at 13.5 MeV. At this energy the calculated cross sections are slightly too low. More measurements of σ_R

[23] B. Wilkins and G. Igo, Phys. Letters **3**, 48 (1962).

[24] H. Budzanowski and K. Grotowski, Phys. Letters **2**, 280 (1962).

are needed to determine whether the discrepancies with the experimental results are significant.

V. DISCUSSION AND CONCLUSIONS

For the two lightest nuclei studied, magnesium and aluminum, the fits are not good and the parameters deviate from the trends of the other nuclei. Several reasons can be found for this behavior. One is that these nuclei are very deformed and one may have to take the

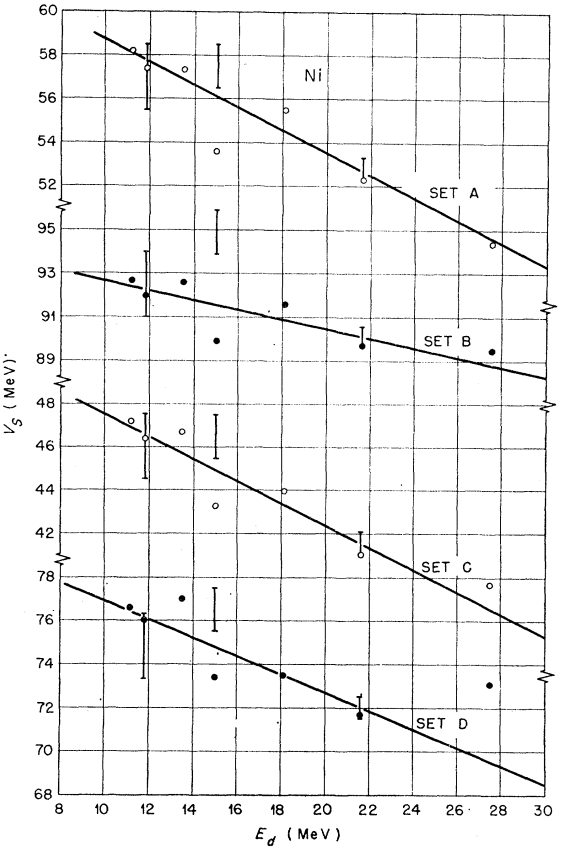

FIG. 19. Real potential well depths, V_S, as a function of energy for the fits to the data for nickel. The potentials were obtained by adjusting the two well depths, V_S and W_D, for the lowest χ^2 when the geometrical parameters were fixed to the values given in Table III. The numerical values of the well depths are given in Appendixes II–V. The relative position of the lines drawn in Fig. 17 for the fits to the 11.8-, 15.0-, and 21.6-MeV data are shown by the vertical bars which are normalized at 21.6 MeV. The length of the bars indicates approximately the spread of the points around the lines on Fig. 17.

excitation of the rotational states into account explicity. Also, the effects of spin-orbit potentials, which we have neglected, are more important for the lighter nuclei, and at 11.8 MeV there may not be sufficient energy averaging in the experimental data to be able to apply the optical model. The fits for calcium at 11.15 and 12.1 MeV were not good, possibly because calcium is a closed shell nucleus. Neither is the fit good for titanium at 11.8 MeV, but at 12.8 MeV it is much

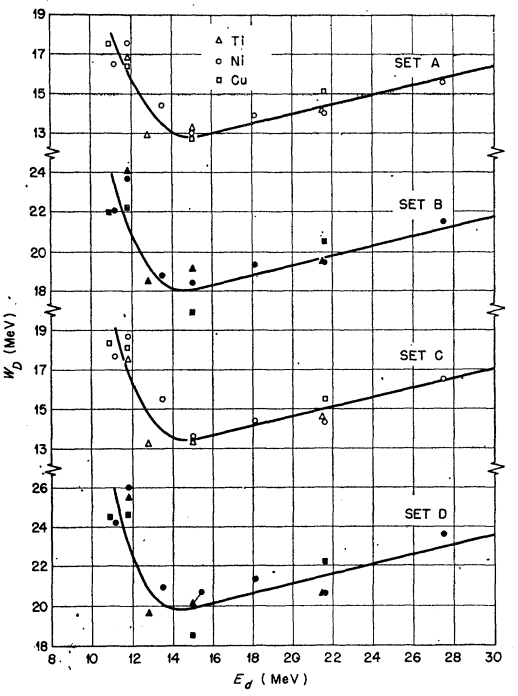

FIG. 20. Surface imaginary potentials, W_D, as a function of energy for the fits to the data for titanium, nickel, and copper. The potentials were obtained by adjusting the two well depths, V_S and W_D, for the lowest χ^2 when the geometrical parameters were fixed to the values given in Table III. The numerical values of the well depths are given in Appendixes II–V.

better. A resonance in one of the partial waves is not at exactly the right energy and explains the difficulty at 11.8 MeV; as one moves slightly away from the resonance, the agreement with the data improves.

It may be very significant that the relative values of the well depths for nickel, copper, and zinc are the same

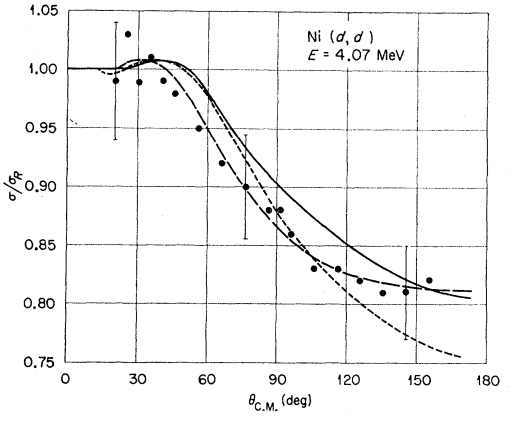

FIG. 21. Comparison of the data at 4.07 MeV for nickel with calculated curves. Solid curve: $V_S=52$ MeV, $W_D=16$ MeV and the geometrical parameters of set C given in Table III; the choice of the well depths is explained in Sec. IV. Dashed curve: well depths are adjusted for the lowest χ^2 ($V_S=129$ MeV, $W_D=72.5$ MeV), when the geometrical parameters of set C are used. Dotted curve: calculated with the parameters of Melkanoff *et al.* (see Ref. 6).

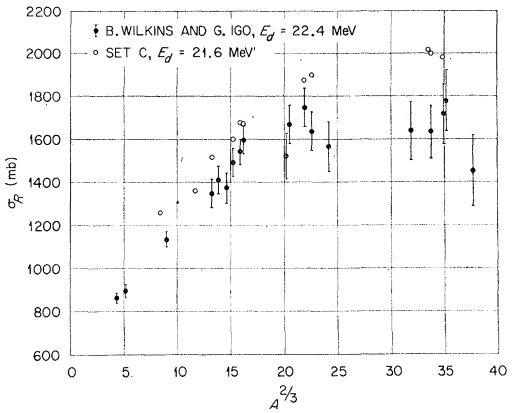

FIG. 22. Comparison of some total reaction cross sections measured at 22.4 MeV with the total reaction cross sections obtained from the analysis of the 21.6-MeV data with the set C geometrical parameters. The numerical values of these theoretical total reaction cross sections are given in Appendix IV.

as in proton scattering.[1] In the case of proton scattering the low value for V_S for nickel was explained by the symmetry energy dependence of the optical model. Such an explanation cannot be given for the case of deuteron scattering and may point to an anomaly for nickel.

The manner in which the average geometrical parameters were determined was quite arbitrary, particulary the choice of the radius parameter r_{0S}. However, we have seen that the qualitative features of the trends in the parameters as a function of mass number and energy are unchanged within the limits of 1.15 and 1.30 F for r_{0S}. On physical grounds the dependence of the radius of the real potential on the mass number could be taken as $R_S=r_{0S}A^{1/3}+\delta$, where δ is related to the size of the deuteron, rather than the term used: $R_S=r_{0S}A^{1/3}$. But the choice we have made will give the smallest A dependence of the real well depth V_S, since we have for deuteron scattering an invariance of the type $V_S R_S{}^n=$constant.

The deuteron elastic scattering data between 11 and 27.5 MeV can be reproduced reasonably well with a simple optical model which shows smooth systematic trends as a function of both mass number and energy. The fact that there are several discrete families of such potentials which fit the data equally well may indicate that the discrete potentials in the interior of the nucleus may only be required to match some boundary condition on the wave function inside the surface of the nucleus and that the surface region of the potential, particularly the tail of the imaginary part of the potential, is of most importance. The optical-model wave function in the interior of the nucleus seems to be characteristic of the model and it is doubtful if any physical significance can be attached to it. However, since the elastic scattering wave function is asymptotically correct, detailed calculations need to be done in the distorted-wave Born approximation for various reactions which are, for the most part, sensitive to different parts of the radial wave function to try to determine how deep inside the nucleus one may assign some physical meaning to the optical model wave function.

ACKNOWLEDGMENTS

It is a pleasure to thank Dr. G. R. Satchler and Dr. B. Buck for many discussions and comments on this work.

APPENDIX I: Results of the search code on fitting all the data by allowing the six parameters to be adjusted for a minimum χ^2.

Energy (MeV)	Element	Type	V_S (MeV)	r_{0S} (F)	a_S (F)	W_D (MeV)	r_{0I} (F)	a_I (F)	σ_R (mb)	χ^2
10.9	Cu	a	60.6	1.111	0.971	14.48	1.468	0.709	1514	0.35
		b	89.5	1.159	0.898	18.81	1.470	0.667	1534	0.39
11.15	Ca	a	65.6	1.000	1.030	13.87	1.519	0.507	1229	2.5
		b	109.1	1.033	0.899	18.73	1.507	0.466	1221	2.9
	Fe	a	51.5	1.156	0.979	15.76	1.433	0.658	1452	0.96
		b	78.5	1.225	0.843	24.11	1.399	0.586	1410	1.3
	Ni	a	50.8	1.237	0.857	15.09	1.433	0.659	1380	0.25
		b	77.3	1.289	0.763	22.55	1.402	0.603	1366	0.32
11.8	Mg	a	35.3	1.151	0.915	15.22	1.470	0.668	1286	3.0
		b	73.1	1.187	0.805	27.7	1.398	0.605	1274	2.5
	Al	a	42.7	1.300[a]	0.868	20.11	1.555	0.475	1210	8.5
		b	57.8	1.563	0.650	50.8	1.558	0.374	1240	9.0
	Ti	a	48.5	1.206	0.815	12.14	1.443	0.668	1380	0.54
		b	72.2	1.335	0.691	21.66	1.403	0.552	1337	1.3
	Fe	a	58.5	1.100	0.864	13.40	1.381	0.718	1385	0.66
		b	95.5	1.112	0.795	19.03	1.325	0.676	1349	0.86
	Ni	a	53.2	1.202	0.869	13.71	1.463	0.667	1432	0.35
		b	76.3	1.305	0.746	20.70	1.424	0.608	1414	0.35
	Cu	a	58.5	1.153	0.879	13.32	1.434	0.708	1476	0.65
		b	90.7	1.172	0.822	18.34	1.410	0.661	1468	0.78
	Zn	a	65.1	1.097	0.851	14.29	1.371	0.761	1451	0.45
		b	103.3	1.083	0.835	19.17	1.354	0.715	1444	0.46
	Zr	a	60.4	1.226	0.733	10.55	1.296	0.812	1319	0.35
		b	85.4	1.272	0.679	18.39	1.236	0.677	1237	0.50
	Nb	a	71.0	1.129	0.754	10.83	1.305	0.755	1195	0.36
		b	95.5	1.201	0.687	18.20	1.240	0.661	1135	0.31

APPENDIX I *(continued)*

Energy (MeV)	Element	Type	V_S (MeV)	r_{0S} (F)	a_S (F)	W_D (MeV)	r_{0I} (F)	a_I (F)	σ_R (mb)	χ^2
	Rb	a	50.5	1.350	0.618	17.99	1.222	0.795	1225	0.64
		b	77.0	1.307	0.639	22.64	1.225	0.728	1199	0.80
	Pd	a	66.2	1.128	0.843	21.36	1.245	0.745	1218	0.09
		b	77.7	1.322	0.654	37.20	1.213	0.617	1173	0.15
	Ag	a	47.1	1.324	0.716	21.96	1.271	0.691	1186	1.1
		b	79.6	1.297	0.664	30.46	1.206	0.661	1147	0.75
	Cd	a	78.1	1.069	0.894	17.10	1.279	0.702	1157	0.20
		b	108.2	1.088	0.843	22.94	1.275	0.646	1149	0.19
	In	a	78.2	1.019	1.021	10.74	1.488	0.781	1515	0.12
		b	113.6	1.003	0.996	13.11	1.467	0.752	1494	0.15
	Sn	a	89.4	0.950[a]	0.635	6.72	1.889	0.801	2265	0.89
		b	110.9	1.000[a]	1.028	11.84	1.560[a]	0.836	1817	1.8
	Ta	a	75.2	1.000[a]	1.066	16.00	1.361	0.777	917	0.38
		b	124.7	1.018	1.002	21.58	1.364	0.701	899	0.40
	Au	a	58.9	1.430	0.577	10.39	1.146	1.058	808	0.47
		b	89.5	1.272	0.723	12.22	1.301	0.877	808	0.47
12.1	Ca	a	56.6	1.116	0.928	14.05	1.494	0.499	1208	7.8
		b	93.5	1.168	0.791	21.55	1.477	0.428	1173	11
12.8	Ti	a	46.7	1.240	0.797	12.24	1.369	0.673	1366	6.7
		b	77.6	1.283	0.706	18.95	1.324	0.622	1377	11
13.5	Ni	a	44.8	1.322	0.816	15.65	1.409	0.652	1502	2.2
		b	70.0	1.378	0.714	25.79	1.403	0.543	1472	2.3
	Sn	a	77.4	1.036	1.060	11.00	1.479	0.812	1820	2.5
		b	73.5	1.385	0.727	22.11	1.357	0.654	1614	3.4
	Au	a	87.9	1.019	1.170	11.84	1.502	0.747	1416	0.76
		b	114.7	1.024	1.135	13.78	1.502	0.718	1415	0.76
15.0	Ti	a	35.84	1.453	0.721	13.66	1.414	0.609	1472	6.2
		b	74.0	1.329	0.710	20.33	1.333	0.645	1514	11
	Fe	a	30.42	1.616	0.679	19.47	1.498	0.432	1528	7.7
		b	64.8	1.448	0.689	26.60	1.412	0.461	1531	16
	*Ni^{58}	a	76.1	0.931	0.840	11.15	1.284	0.850	1484	1.0
		b	98.6	1.105	0.709	16.49	1.170	0.831	1436	1.1
	Cu	a	73.3	0.982	1.118	14.70	1.409	0.710	1722	5.2
		b	105.1	1.070	0.962	20.25	1.366	0.668	1690	6.8
	*Zr	a	68.1	1.098	0.911	11.66	1.404	0.682	1572	0.63
		b	98.1	1.127	0.848	14.87	1.394	0.655	1595	0.71
	Rh	a	78.5	0.996	1.036	12.02	1.453	0.877	2028	1.9
		b	110.5	1.028	0.973	15.11	1.409	0.853	1981	1.9
	Pd	a	68.1	1.114	0.864	9.97	1.470	0.908	2035	2.7
		b	103.2	1.093	0.850	12.41	1.409	0.904	1993	2.7
	Sn	a	77.5	0.994	1.160	12.54	1.535	0.771	2061	2.3
		b	109.3	1.013	1.071	14.54	1.505	0.768	2043	2.6
	*Sn^{120}	a	75.3	1.104	0.688	10.29	1.247	0.940	1582	0.65
		b	99.7	1.168	0.611	12.14	1.213	0.985	1680	0.83
	Ta	a	49.3	1.469	0.669	24.69	1.437	0.540	1473	2.3
		b	84.2	1.303	0.733	26.41	1.343	0.653	1416	3.1
	*Au	a	86.7	1.054	0.789	6.93	1.370[a]	1.032	1595	0.07
		b	103.7	1.123	0.839	11.08	1.340[a]	0.916	1529	0.08
	Au	a	89.7	1.011	1.113	13.09	1.455	0.693	1477	1.5
		b	77.0	1.363	0.763	22.92	1.442	0.561	1435	1.7
	Pb	a	93.4	0.986	1.184	12.43	1.484	0.621	1406	1.7
		b	133.4	0.930	1.175	12.80	1.500	0.623	1445	1.8
18.1	Ni^{60}	a	73.5	0.926	1.072	14.51	1.415	0.710	1709	2.8
		b	126.9	0.904	0.987	18.09	1.383	0.707	1714	3.4
21.6	Mg	a	38.30	1.000	0.972	17.70	1.360	0.694	1278	62
		b	61.2	1.416	0.571	17.40	1.088	0.847	1291	45
21.4	Ca^{40}	a	45.0	1.287	0.590	5.71	1.195	1.075	1462	17
		b	98.5	1.070	0.931	20.27	1.570	0.483	1486	19
21.5	Ti^{48}	a	65.6	0.909	1.068	14.08	1.419	0.685	1613	3.6
		b	106.0	0.997	0.916	18.33	1.400	0.643	1599	9.3
21.6	Ni	a	56.3	1.093	0.923	14.37	1.377	0.689	1629	6.9
		b	101.4	1.064	0.856	19.52	1.330	0.683	1640	5.0
	Cu	a	68.3	0.984	1.049	17.15	1.373	0.668	1709	9.3
		b	102.8	1.055	0.892	21.06	1.348	0.676	1735	9.2
	Zn	a	61.6	1.071	0.973	16.42	1.345	0.709	1732	11
		b	106.5	1.038	0.886	20.32	1.307	0.736	1765	6.6
	Rh	a	63.6	1.130	0.882	18.26	1.283	0.705	1793	2.4
		b	94.2	1.160	0.778	25.20	1.230	0.676	1747	3.2
	Ag	a	67.8	1.095	0.910	18.61	1.270	0.704	1785	2.3
		b	97.8	1.133	0.800	25.47	1.220	0.680	1748	2.8
	Pt	a	78.7	1.069	1.005	14.84	1.364	0.819	2233	1.2
		b	78.2	1.328	0.722	27.67	1.292	0.663	2041	1.9

APPENDIX I (*continued*)

Energy (MeV)	Element	Type	V_S (MeV)	r_{0S} (F)	a_S (F)	W_D (MeV)	r_{0I} (F)	a_I (F)	σ_R (mb)	χ^2
	Au	a	82.0	1.046	1.018	13.87	1.360	0.804	2161	0.87
		b	82.3	1.303	0.731	27.29	1.289	0.638	1967	1.9
	Pb^{206}	a	74.2	1.137	0.892	11.84	1.334	0.796	2015	1.0
		b	93.7	1.194	0.796	15.63	1.291	0.758	1960	1.4
27.5	Ni^{58}	a	53.9	1.101	0.978	16.51	1.437	0.600	1654	2.4
		b	81.6	1.234	0.776	23.49	1.404	0.559	1641	2.9

[a] Value of parameter not adjusted by code.

APPENDIX II: Values of the well depths obtained by using the set A geometrical parameters of Table III. (The well depths were adjusted for the lowest χ^2 in fitting each angular distribution.)

Energy (MeV)	Element	V_S (MeV)	W_D (MeV)	σ_R (mb)	χ^2
10.9	Cu	62.0	16.5	1372	0.71
11.15	Ca	52.8	16.5	1337	20
	Fe	54.9	14.1	1354	3.0
	Ni	58.2	16.5	1355	0.55
11.8	Mg	36.3	19.4	1274	6.2
	Al	35.4	24.2	1342	48
	Ti	51.5	16.8	1420	12
	Fe	54.6	15.2	1400	2.1
	Ni	57.4	17.6	1403	3.4
	Cu	59.9	16.4	1429	1.9
	Zn	60.4	16.7	1421	1.3
	Zr	66.6	12.0	1334	2.4
	Nb	64.7	14.9	1334	4.1
	Rh	64.3	17.2	1297	2.2
	Pd	66.2	15.3	1283	0.82
	Ag	66.1	15.5	1262	1.4
	Cd	69.5	13.5	1253	0.64
	In	71.0	12.4	1230	1.7
	Sn	73.7	11.4	1228	8.9
	Ta	83.5[a]	11.0	787	1.3
	Au	85.7	7.46	622	2.1
12.1	Ca	54.6	16.6	1377	53
12.8	Ti	52.8	12.9	1419	9.0
13.5	Ni	57.3	14.4	1458	3.2
	Sn	72.1	10.9	1415	9.8
	Au	86.2	7.64	964	15
15.0	Ti	53.5	13.2	1479	12
	Fe	56.5	11.7	1484	46
	*Ni^{58}	53.6	13.0	1476	2.5
	Cu	62.1	12.7	1544	36
	*Zr	64.4	12.7	1575	1.1
	Rh	74.2	12.8	1578	31
	Pd	73.2	12.6	1578	21
	Sn	70.9	12.5	1565	12
	*Sn^{120}	68.5	12.7	1572	1.8
	Ta	78.4	15.0	1366	3.5
	*Au	81.1	10.3	1232	1.2
	Au	78.9	11.1	1237	5.2
	Pb	82.2	11.5	1209	8.9
18.1	Ni^{60}	55.5	13.9	1596	11
21.6	Mg	33.3	16.7	1278	67
21.4	Ca^{40}	53.5	9.29	1374	44
21.5	Ti^{48}	49.3	14.1	1560	10
21.6	Ni	52.3	14.0	1623	9.2
	Cu	54.7	15.1	1695	16
	Zn	55.8	14.2	1691	27
	Rh	62.2	13.9	1857	23
	Ag	62.9	13.7	1868	29
	Pt	79.0	12.1	1943	44
	Au	77.7	11.7	1923	38
	Pb^{206}	75.8	10.2	1883	14
27.5	Ni^{58}	49.4	15.6	1681	5.7

[a] Value of parameter not adjusted by code.

APPENDIX III: Values of the well depths obtained by using the set B geometrical parameters of Table III. (The well depths were adjusted for the lowest χ^2 in fitting each angular distribution.)

Energy (MeV)	Element	V_S (MeV)	W_D (MeV)	σ_R (mb)	χ^2
10.9	Cu	97.0	22.0	1372	1.0
11.15	Ca	91.2	23.4	1372	22
	Fe	90.0	19.3	1375	3.5
	Ni	92.7	22.1	1358	0.84
11.8	Mg	67.9	27.4	1314	9.7
	Ti	86.6	24.1	1444	14
	Fe	89.1	20.9	1418	2.1
	Ni	92.0	23.7	1406	4.2
	Cu	94.6	22.2	1432	2.8
	Zn	94.8	22.5	1420	1.9
	Zr	98.3	15.5	1322	1.0
	Nb	96.3	18.9	1314	2.9
	Rh	91.8	19.9	1253	1.3
	Pd	97.7	18.7	1259	1.1
	Ag	97.0	18.7	1230	1.4
	Cd	100.9	16.4	1224	0.96
	In	101.5	15.0	1205	2.8
	Sn	104.0	13.0	1196	12
	Ta	111.0[a]	11.3	735	2.6
	Au	115.7	7.56	582	4.4
12.1	Ca	95.8	22.1	1410	58
12.8	Ti	90.2	18.5	1458	15.
13.5	Ni	92.6	18.8	1469	3.4
	Sn	102.5	13.4	1389	13
	Au	112.9	8.45	916	22
15.0	Ti	92.2	19.1	1523	13
	Fe	94.4	15.9	1520	40
	*Ni^{58}	89.9	18.4	1508	2.5
	Cu	99.1	16.9	1560	34
	*Zr	97.0	16.2	1567	1.1
	Rh	107.0	16.4	1559	35
	Pd	105.7	15.9	1561	24
	Sn	101.8	15.6	1538	16
	*Sn^{120}	99.1	15.9	1545	1.6
	Ta	107.5	17.1	1310	4.6
	*Au	109.0	11.9	1183	2.0
	Au	106.9	12.9	1183	7.4
	Pb	107.7	12.5	1145	11
18.1	Ni^{60}	91.6	19.3	1621	14
21.6	Mg	88.1	17.5	1310	72
21.4	Ca^{40}	93.0	23.1	1543	74
21.5	Ti^{48}	88.3	19.4	1598	17
21.6	Ni	89.7	19.4	1655	7.9
	Cu	91.2	20.5	1715	13
	Zn	91.7	19.4	1711	35
	Rh	95.1	17.9	1847	39
	Ag	95.4	17.6	1855	50
	Pt	107.5	14.8	1895	66
	Au	104.3	14.4	1875	55
	Pb^{206}	103.2	12.7	1843	20
27.5	Ni^{58}	89.5	21.5	1714	6.1

[a] Value of parameter not adjusted by code.

APPENDIX IV: Values of the well depths obtained by using the set C geometrical parameters of Table III. (The well depths were adjusted for the lowest χ^2 in fitting each angular distribution.)

Energy (MeV)	Element	V_S (MeV)	W_D (MeV)	σ_R (mb)	χ^2
10.9	Cu	50.5	18.3	1373	0.81
11.15	Ca	43.8	16.7	1313	21
	Fe	44.7	14.9	1347	3.0
	Ni	47.2	17.7	1346	0.58
11.8	Mg	32.3	19.8	1238	6.0
	Al	32.6	25.6	1310	45
	Ti	41.8	17.5	1400	14
	Fe	43.7	15.9	1386	3.0
	Ni	46.4	18.7	1390	3.6
	Cu	48.4	18.1	1426	2.8
	Zn	48.5	18.4	1418	1.6
	Zr	52.6	14.2	1360	2.3
	Nb	51.4	17.9	1359	5.4
	Rh	47.4	19.1	1300	2.3
	Pd	54.1	19.2	1324	1.0
	Ag	50.4	17.8	1280	1.6
	Cd	54.9	17.3	1297	0.67
	In	56.1	16.0	1279	1.0
	Sn	58.5	14.5	1280	6.5
	Ta	71.2	21.6	899	0.39
	Au	67.0	13.7	725	0.56
12.1	Ca	46.2	15.8	1349	58
12.8	Ti	42.9	13.2	1404	11
13.5	Ni	46.7	15.5	1455	2.8
	Sn	58.1	13.3	1473	6.4
	Au	67.1	11.4	1077	5.7
15.0	Ti	43.6	13.4	1462	9.2
	Fe	45.4	12.1	1477	38
	*Ni^{58}	43.3	13.6	1468	2.6
	Cu	49.7	13.5	1543	37
	*Zr	51.4	14.6	1600	2.1
	Rh	57.6	14.6	1608	19
	Pd	56.9	14.4	1612	13
	Sn	56.2	14.9	1612	8.5
	*Sn^{120}	54.2	15.4	1619	2.2
	Ta	61.9	22.8	1453	2.7
	*Au	63.6	14.5	1335	0.24
	Au	62.8	17.2	1345	2.9
	Pb	62.4	19.0	1316	6.4
18.1	Ni^{60}	44.0	14.4	1582	16
21.6	Mg	29.6	18.4	1261	90
21.4	Ca^{40}	42.9	9.6	1362	45
21.5	Ti^{48}	40.0	14.6	1540	17
21.6	Ni	41.1	14.3	1602	25
	Cu	43.5	15.5	1677	23
	Zn	43.8	14.5	1672	38
	Rh	49.2	15.3	1876	15
	Ag	50.6	15.3	1895	15
	Pt	59.0	14.6	2017	9.7
	Au	58.0	14.3	2001	31
	Pb^{206}	58.0	13.1	1983	4.8
27.5	Ni^{58}	39.7	16.5	1664	5.7

APPENDIX V: Values of the well depths obtained by using the set D geometrical parameters of Table III. (The well depths were adjusted for the lowest χ^2 in fitting each angular distribution.)

Energy (MeV)	Element	V_S (MeV)	W_D (MeV)	σ_R (mb)	χ^2
10.9	Cu	80.0	24.5	1379	1.1
11.15	Ca	77.6	23.1	1351	21
	Fe	74.2	20.9	1376	3.6
	Ni	76.6	24.2	1360	0.74
11.8	Mg	60.8	28.3	1281	7.1
	Ti	71.9	25.5	1432	14
	Fe	73.3	22.8	1417	2.4
	Ni	76.0	26.0	1406	4.0
	Cu	77.5	24.6	1437	3.1
	Zn	77.5	25.1	1427	1.0
	Zr	79.1	18.6	1362	1.6
	Nb	78.0	23.4	1352	4.3
	Rh	73.5	25.2	1292	1.7
	Pd	79.1	23.9	1309	0.87
	Ag	76.6	23.4	1271	1.2
	Cd	80.5	21.4	1278	0.55
	In	81.4	19.7	1264	1.3
	Sn	83.5	17.6	1259	8.4
	Ta	97.0	22.9	857	0.47
	Au	92.0	14.5	693	1.4
12.1	Ca	80.7	20.9	1386	54
12.8	Ti	74.8	19.6	1454	17
13.5	Ni	77.0	20.9	1479	3.1
	Sn	83.3	17.0	1460	9.0
	Au	89.9	13.1	1041	9.0
15.0	Ti	76.5	20.1	1519	11
	Fe	77.7	17.4	1529	41
	*Ni^{58}	73.4	20.1	1512	3.1
	Cu	80.7	18.5	1574	34
	*Zr	78.5	19.2	1609	1.9
	Rh	84.6	19.4	1605	23
	Pd	83.6	19.2	1611	15
	Sn	82.0	19.8	1604	10
	*Sn^{120}	79.5	20.1	1608	1.8
	Ta	85.3	26.9	1407	3.1
	*Au	86.2	17.0	1295	0.52
	Au	85.2	19.9	1299	3.9
	Pb	84.6	21.6	1265	7.7
18.1	Ni^{60}	73.5	21.3	1623	25
21.6	Mg	69.0	19.3	1285	61
21.4	Ca^{40}	78.0	12.8	1425	37
21.5	Ti^{48}	72.1	20.6	1590	28
21.6	Ni	71.7	20.6	1650	22
	Cu	73.1	22.2	1714	29
	Zn	72.9	20.9	1712	58
	Rh	76.2	21.0	1888	32
	Ag	77.4	20.7	1904	36
	Pt	83.0	19.1	1995	15
	Au	81.3	18.5	1977	35
	Pb^{206}	80.7	16.8	1959	5.6
27.5	Ni^{58}	73.1	23.6	1713	6.5